International Forum on Aeroelasticity and Structural Dynamics
IFASD 2022
13-17 June 2022, Madrid, Spain

ESTIMATION OF GLOBAL STRUCTURAL AIRCRAFT LOADS DUE TO ATMOSPHERIC DISTURBANCES FOR STRUCTURAL FATIGUE ESTIMATION

Simon Schulz[1] **and Daniel Ossmann**[2]

[1]Institute of System Dynamics & Control
German Aerospace Center (DLR), 82234 Wessling, Germany
simon.schulz@dlr.de

[2]Department of Mechanical, Automotive and Aerospace Engineering,
Munich University of Applied Sciences HM, 80335 Munich, Germany
daniel.ossmann@hm.edu

Keywords: Loads estimation, Kalman-Bucy Filter, Discrete Gust, Continuous Turbulence, Equivalent Damage Load, Aeroelasticity.

Abstract: An approach to estimate global structural loads caused by atmospheric disturbances from recorded sensor data of operational flights is presented in this paper. The presented approach is based on augmenting a dynamic, flexible aircraft model with disturbance dynamics. A state observer for this augmented model, i.e., a Kalman-Bucy filter, is derived. The sensor-data is processed through the observer, enabling the estimation of the encountered atmospheric disturbances by the aircraft. Subsequently, these estimated disturbances are used to estimate the global aircraft loads. In order to evaluate the load estimation results, the concept of equivalent damage load is applied. It connects the global loads to their influence on the aircraft's structural fatigue. For verification of the proposed toolchain, design scenarios from certification, i.e., discrete gust and continuous turbulence encounters, are simulated to emulate real operational data. The gathered data is used to compare the resulting estimated loads to the simulated loads with respect to the equivalent damage loads.

1 INTRODUCTION

For civil aircraft operators a main motivation is to decrease direct operating cost (DOC) without compromising safety and reliability. Possibilities to achieve this are, e.g., reducing aircraft weight or reducing the inspection effort [1]. These two measures, however, are contradicting each other, since reduction in weight ultimately leads to reduced margins against structural failures, which subsequently requires more frequent inspections and therefore higher inspection costs [1]. In [1], one aspect to decrease the latter is to increase the information about the aircraft structure during operation. The chain of cause for fatigue damage due to structural loads is described by Schmuecker in [2]. He details, that all structural loads result from operational and environmental conditions, which lead to internal stresses. These stresses result in fatigue in the components, which is one reason for structural damage. Consequently, in this paper the focus lies on gathering information about a main cause for structural fatigue, namely atmospheric disturbances occurring during aircraft operation. In the literature different approaches for the operational loads estimation for civil and military application, also named operational loads monitoring (OLM), can be found. In the military domain, one system is implemented in the

Eurofighter Typhoon. The system monitors multiple locations on the structure. The monitoring is either based on sensor data already available for different subsystem of the aircraft, e.g, the flight control system, or based on specifically installed sensors for the monitoring, e.g., strain gauges [3]. The military applications are not further considered herein, since the approach in this paper is oriented towards civil aircraft for which no additional sensors should be installed. The ideas of an operational load monitoring system (OLMS) goes back to [2]. In this approach a dynamic aircraft model together with data provided by the avionic system is used to monitor the loads. The basic architecture of the approach described herein is based on the ideas from [4]. It combines an integrated rigid body with a structural dynamic aircraft model and augments the resulting system with a disturbance model. The state observer finally uses data provided by the flight control system. Lately, this approach has been enhanced to a hybrid loads estimator via local neural networks in [5], showing promising results and providing that the basic ideas from [4] can be further exploited. The approach in this paper consists of three main components, as illustrated in Figure 1. Starting point is the recorded data from the operational flight mission. Modeling constraints require the recorded data to be sectioned into time frames, where the assumption of constant Mach-number, dynamic pressure as well as constant aircraft mass holds. The sensor data y consists of flight parameters, which are also used by the electronic flight control system. Hence no additional sensors are needed. Furthermore, control surface deflections and thrust commands, summarized in the input vector u, are required.

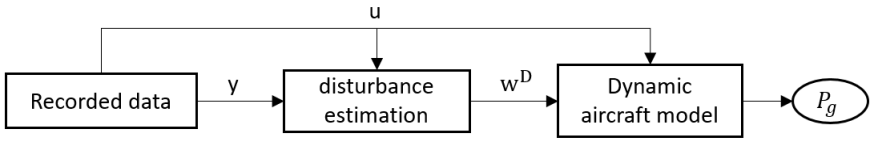

Figure 1: Approach for cut loads estimation due to disturbances from recorded data

The method to design the disturbance estimator shown in Figure 1 is detailed in Section 2. Section 3 defines the dynamic, flexible aircraft model required for the filter. Subsequently, Section 4 introduces the concept of equivalent damage loads (EDL) for fatigue analysis. Finally, Section 5 applies the described toolchain to a realistic aircraft model in order to verify the proposed method.

2 OBSERVER BASED DISTURBANCE ESTIMATION

The estimation of the atmospheric disturbances, described by a wind signal, is required for the estimation of the global structural loads. The disturbance estimator is based on a classic observer architecture. The filter is designed applying the Kalman-Bucy method. This section is divided in the underlying theory of the filter design and the augmentation of this architecture by the disturbance model in order to estimate unknown input disturbances.

2.1 Kalman-Bucy filter

The architecture of the Kalman-Bucy filter is displayed as a block diagram in Figure 2. The block ”System” represents the real system and y the measurement data from the sensors. The control inputs are described by u. The signals ν and w characterize the process respectively sensor noise. Both signals are assumed to be uncorrelated white noise with zero mean. The observer contains a ”System Model”, which represents the ”System”´s dynamics by a linear state space model. The block L represents the feedback gain of the observer which processes the error e between the measurements of the real system y and the estimated measurements of the system model $\hat{y}$. The resulting signal is fed into the ”System Model” in order to minimize e.

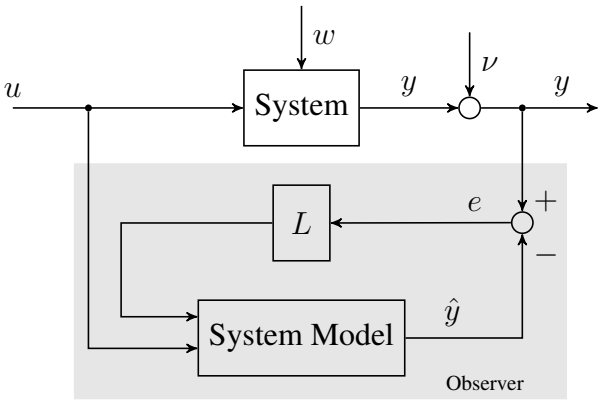

Figure 2: General Observer architecture

The feedback gain L represents the tuning parameter of this architecture. It is derived applying the method defined by the Kalman-Bucy filter [6]. For the design process the model of the block "System" is represented by:

$$\begin{aligned} \dot{x} &= Ax + Bu + w \\ y &= Cx + Du + \nu \\ w(t) &\sim (0, Q) \\ \nu(t) &\sim (0, R) \\ E[\nu_k w_j^T] &= 0. \end{aligned} \tag{1}$$

The matrices Q and R describe the covariance matrices of the process and sensor noise. A Kalman-Bucy filter for this model is defined as

$$\dot{\hat{x}} = (A - LC)\hat{x} + Bu + Ly \tag{2}$$

where the system state estimate is given by $\hat{x}$. The design of the feedback gain L is based on minimizing the sum of the variances of the error between the system states x and the estimated states $\hat{x}$. Hence, the cost function

$$\begin{aligned} J &= \lim_{t\to\infty} E[(x_1(t) - \hat{x}_1(t))^2)] + ... + E[(x_n(t) - \hat{x}_n(t))^2)] \\ &= \lim_{t\to\infty} E[(x(t) - \hat{x}(t))^T (x(t) - \hat{x}(t))] \\ &= \lim_{t\to\infty} Tr(P), \end{aligned} \tag{3}$$

needs to be minimized with respect to L in (2) [6]. The covariance of the estimation error P and its evolution is described by the solution of the differential Riccati equation (4) [6].

$$\dot{P} = -PC^T R^{-1} CP + AP + PA^T + Q. \tag{4}$$

Under the assumption that A, C, Q, R are constant, P can reach steady state value. The steady value of P can be derived using the algebraic Riccati equation (ARE) or continuous ARE (CARE):

$$AP + PA^T - PC^T R^{-1} CP + Q = 0. \tag{5}$$

Based on the steady state solution of (5), the feedback gain L to minimize (3) is given by

$$L = PC^T R^{-1}. \tag{6}$$

2.2 Disturbance estimator

The focus of this paper lies on the estimation of loads due to external atmospheric disturbances. Since the disturbance is not measurable, it needs to be estimated using the previously described Kalman-Bucy filter. For the derivation of the disturbance estimator the general linear system dynamics model in state space representation is given by:

$$\begin{aligned} \dot{x} &= Ax + B_1 u + B_2 d \\ y &= Cx + D_1 u + D_2 d. \end{aligned} \tag{7}$$

The disturbance input d is unknown. In order to estimate the unknown disturbance, the system model is extended by an additional model which represents the dynamics of the unknown disturbance. The corresponding disturbance model is defined as

$$\begin{aligned} \dot{x}_d &= A_d \cdot x_d \\ d &= C_d \cdot x_d. \end{aligned} \tag{8}$$

The extended or augmented model results in an extended general disturbance estimator structure as displayed in Figure 3. Since the disturbance itself is unknown, the model defined in (8) has no input. The augmentation of the standard system model (7) with (8) by connecting the output of the disturbance model to the input of the system model leads to the following augmented system model:

$$\begin{aligned} \begin{bmatrix} \dot{x} \\ \dot{x}_d \end{bmatrix} &= \begin{bmatrix} A & B_2 C_d \\ 0 & A_d \end{bmatrix} \begin{bmatrix} x \\ x_d \end{bmatrix} + \begin{bmatrix} B_1 \\ 0 \end{bmatrix} u \\ \begin{bmatrix} y \\ d \end{bmatrix} &= \begin{bmatrix} C & D_2 C_d \\ 0 & C_d \end{bmatrix} \begin{bmatrix} x \\ x_d \end{bmatrix} + \begin{bmatrix} D_1 \\ 0 \end{bmatrix} u. \end{aligned} \tag{9}$$

The Kalman-Bucy filter estimates the model states $\hat{x}$ as well as the states of the disturbance model $\hat{x}_d$. Both are corrected due to the error e represented by the signals ξ_m and ξ_d, which are defined as

$$\begin{bmatrix} \xi_m \\ \xi_d \end{bmatrix} = L \cdot e. \tag{10}$$

Thus, the disturbance estimate is given by $\hat{d} = C_d \hat{x}_d$. For the application in this paper the disturbance model depicted in (9) and Figure 3 is simplified by assuming a constant disturbance which translates to $A_d = 0$. This leads to an open loop integrator for the disturbance model, i.e.

$$\begin{aligned} \begin{bmatrix} \dot{x} \\ \dot{x}_d \end{bmatrix} &= \begin{bmatrix} A & B_2 C_d \\ 0 & 0 \end{bmatrix} \begin{bmatrix} x \\ x_d \end{bmatrix} + \begin{bmatrix} B_1 \\ 0 \end{bmatrix} u \\ \begin{bmatrix} y \\ d \end{bmatrix} &= \begin{bmatrix} C & D_2 C_d \\ 0 & C_d \end{bmatrix} \begin{bmatrix} x \\ x_d \end{bmatrix} + \begin{bmatrix} D_1 \\ 0 \end{bmatrix} u. \end{aligned} \tag{11}$$

The system model with this simplified disturbance model is shown in Figure 4. Based on the simplified augmented model (4), the Kalman-Bucy filter is designed according to the method presented in Section 2.1. The model equations for the design of the filter are

$$\begin{aligned} \begin{bmatrix} \dot{x} \\ \dot{x}_d \end{bmatrix} &= \begin{bmatrix} A & B_2 C_d \\ 0 & 0 \end{bmatrix} \begin{bmatrix} x \\ x_d \end{bmatrix} + \begin{bmatrix} B_1 \\ 0 \end{bmatrix} u + \begin{bmatrix} w \\ w_d \end{bmatrix} \\ \begin{bmatrix} y \\ d \end{bmatrix} &= \begin{bmatrix} C & D_2 C_d \\ 0 & C_d \end{bmatrix} \begin{bmatrix} x \\ x_d \end{bmatrix} + \begin{bmatrix} D_1 \\ 0 \end{bmatrix} u + \begin{bmatrix} \nu \\ 0 \end{bmatrix} \end{aligned} \tag{12}$$

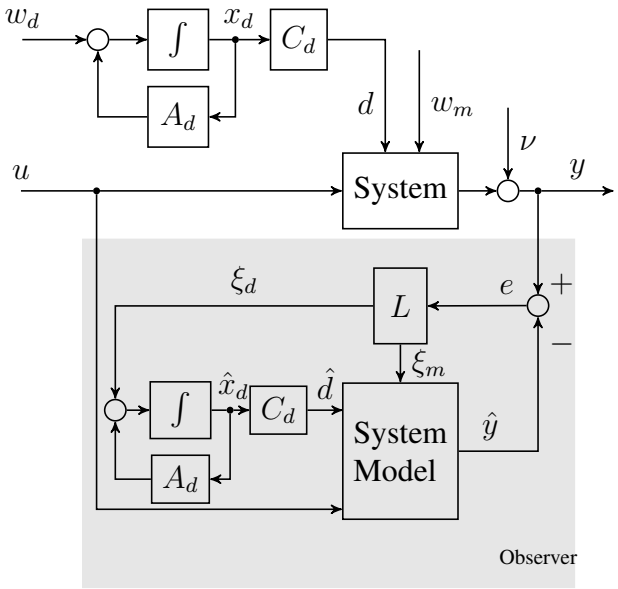

Figure 3: General disturbance estimator structure

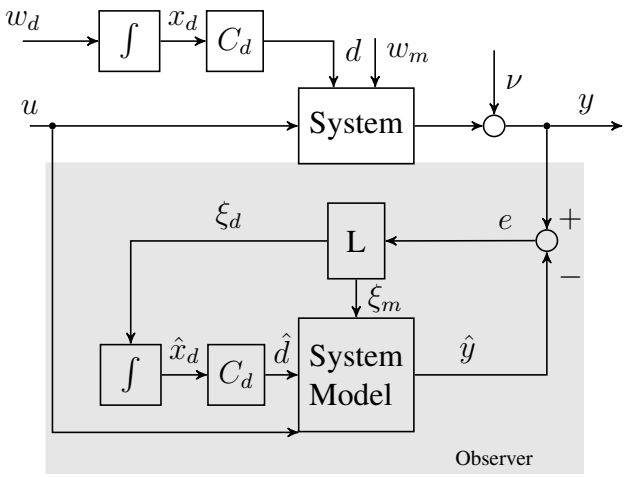

Figure 4: General disturbance estimator structure with simplified disturbance model

where w consists of the system model process noise w_m and the disturbance process noise w_d. The Kalman-Bucy filter for disturbance estimation is given in the following equations:

$$\begin{aligned}\begin{bmatrix}\dot{\hat{x}}\\ \dot{\hat{x}}_d\end{bmatrix} &= \begin{bmatrix}A & B_2C_d\\ 0 & 0\end{bmatrix}\begin{bmatrix}\hat{x}\\ \hat{x}_d\end{bmatrix} + \begin{bmatrix}B_1\\ 0\end{bmatrix}u + L(y-\hat{y})\\ \begin{bmatrix}\hat{y}\\ \hat{d}\end{bmatrix} &= \begin{bmatrix}C & D_2C_d\\ 0 & C_d\end{bmatrix}\begin{bmatrix}\hat{x}\\ \hat{x}_d\end{bmatrix} + \begin{bmatrix}D_1\\ 0\end{bmatrix}u.\end{aligned} \tag{13}$$

3 AEROELASTIC MODELING

The "System Model" within the observer describes a dynamic, flexible aircraft. It is derived using the Varloads (Variable Loads Environment) framework [7]. The system model, in linear state space form, is derived from a non-linear system description. The rigid body dynamics of the aeroelastic aircraft are described by non-linear Newton-Euler equations of motion, while the structural dynamics are represented by second order differential equations:

$$\begin{aligned}\begin{bmatrix}m_b\left(\dot{V}_b + \Omega_b \times V_b - T_{bE}\cdot g_E\right)\\ J_b\dot{\Omega}_b + \Omega_b \times (J_b\Omega_b)\end{bmatrix} &= \Phi_{gb}^T P_g^{ext}\\ M_{ff}\ddot{u}_f + B_{ff}\dot{u}_f + K_{ff}u_f &= \Phi_{gf}^T P_g^{ext}.\end{aligned} \tag{14}$$

The translational and angular velocity of the aircraft center of mass in body axis (index b) are defined by $V_b = \begin{bmatrix}u_b & v_b & w_b\end{bmatrix}$ respectively $\Omega_b = \begin{bmatrix}p_b & q_b & r_b\end{bmatrix}$. The structural dynamics are represented by the modal deformations u_f, velocities $\dot{u}_f$ and accelerations $\ddot{u}_f$. The modal structural dynamics are defined by mass M_{ff}, damping B_{ff} and stiffness K_{ff} matrices. The corresponding modal transformation matrices are Φ_{gb} and Φ_{gf}. The external loads P_g^{ext} consist of the aerodynamic P_g^{aero} and propulsion loads P_g^{prop} on the structural grid (index g). The aerodynamic loads are modeled by panel methods, steady vortex lattice method (VLM) or unsteady doublet lattice method (DLM), which are based on potential flow theory. The aerodynamic load

equation for the VLM model is defined as:

$$P_g^{aero} = q_\infty T_{kg}^T S_{kj} \underbrace{Q_{jj} w_j}_{\Delta c_p}, \tag{15}$$

where q_∞ is the freestream dynamic pressure and T_{kg} the so-called splining matrix, which maps the displacement of the structural grid to the aerodynamic panel model and vice versa the aerodynamic loads to the structural grid. S_{kj} integrates the pressure coefficients Δc_p over each panel j. The pressure coefficients depend on the aerodynamic influence coefficient (AIC) matrix Q_{jj} as well as the downwash w_j, normalized by the freestream velocity U_∞. For the DLM, the AIC matrix depends on the reduced frequency k:

$$\Delta c_p(k) = Q_{jj}(k) w_j(k). \tag{16}$$

For more detailed information on the DLM, the reader is referred to [8].
The Kalman-Bucy filter requires the model in linear state space form. Hence the model defined in (14) needs to be linearized. The equation (14) can be represented more generally as

$$\begin{aligned} \dot{x} &= f(x,u) \\ y &= g(x,u) \end{aligned} \tag{17}$$

in order to explain the linearization process. First, the non-linear model is trimmed for a 1g steady horizontal flight. This results in required trim states x_0 and the trim point corresponding control inputs u_0. The linearized model is derived by a first order Taylor approximation

$$\begin{aligned} A &= \left.\frac{\delta f}{\delta x}\right|_{x_0,u_0} & B &= \left.\frac{\delta f}{\delta u}\right|_{x_0,u_0} \\ C &= \left.\frac{\delta g}{\delta x}\right|_{x_0,u_0} & D &= \left.\frac{\delta g}{\delta u}\right|_{x_0,u_0} \end{aligned} \tag{18}$$

resulting in the state space matrices A, B, C, D.

3.1 Load recovery

In order to obtain the structural loads P_g at the nodes of the structural grid (g-set), the application of the Force Summation Method [8] is necessary, since the model defined in (14) is defined in modal coordinates. To derive the nodal loads P_g the load recovery equation is defined by:

$$P_g = P_g^{ext} - P_g^{iner} = P_g^{aero} + P_g^{prop} - P_g^{iner} \tag{19}$$

where P_g^{ext} are the external loads and P_g^{iner} are the intertia loads defined by

$$P_g^{iner} = M_{gg} \left\{ \Phi_{gb} \ddot{u}_b + \Phi_{gf} \ddot{u}_f \right\}. \tag{20}$$

The inertia loads depend on the modal accelerations $\ddot{u}_f$ and $\ddot{u}_b$, which are given by

$$\ddot{u}_g = \begin{bmatrix} (\dot{V}_b + \Omega_b \times V_b - T_{bE}\, g_E) \\ \dot{\Omega}_b + J_b^{-1} \left(\Omega_b \times (J_b \Omega_b) \right) \end{bmatrix}. \tag{21}$$

The nodal loads P_g are processed in a next step to derive the internal structural loads (cut loads) [9]

$$P_c = T_{cg} \cdot P_g, \tag{22}$$

where T_{cg} is the transformation matrix from nodal loads to cut loads.

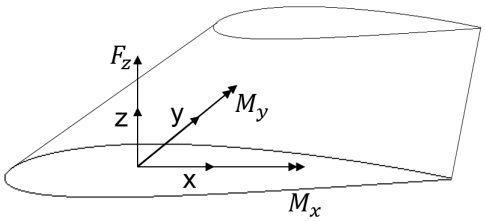

Figure 5: Internal loads coordinate system

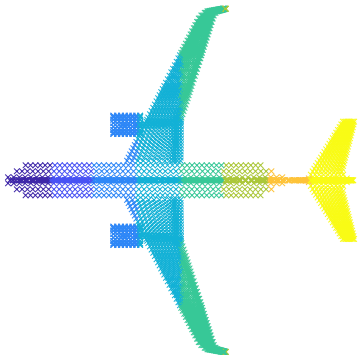

Figure 6: Top view of gust zones

3.2 Atmospheric disturbance model

The disturbance estimation approach is based on augmenting the dynamic aeroelastic aircraft model by the dynamics of the disturbance [4]. Aerodynamic loads due to external atmospheric disturbance are modeled according to (15) with the downwash w_j being equal to the downwash of the atmospheric disturbance atmospheric disturbance w_j^G. Hence the aerodynamic loads due to atmospheric disturbance only depend on w_j^G, which is a vector with dimension $n_j \times 1$ with n_j being the number of panels. The disturbance estimation requires a reduction of the input dimension to 1. In order to reduce the input dimension of the disturbance, the aerodynamic panel model of the aircraft is divided into multiple zones as displayed in Figure 6, where each color represents one zone. Within each zone l, the same downwash w_l is assumed. This zone-wise downwash is transformed to each panel by the transformation matrix T_{jl}. Mathematically, this is described by

$$w_j^G = T_{jl} \cdot w_l^G. \tag{23}$$

To further reduce dimension of disturbance input from number of zones to only one signal w^G, it is assumed, that the disturbance is a spanwise equally distributed and the aircraft flies through the disturbance. Hence the process of flying through the disturbance can be modelled by the different zones experiencing the same disturbance in magnitude and direction, only delayed depending on the true airspeed V_{TAS}. This delay is modeled by the system $G^{delay}(s)$. The delay between the gust zones is modeled by a state space system $G^{delay}(s)$, which consists of multiple Padé-filters, where each Padé-filter describes the delay of the signal from gust zone l to gust zone $l+1$. A time delay in frequency domain can be modeled according to [10] by:

$$G^{\text{delay}}(s) = e^{-sT}, \tag{24}$$

where T describes the time delay in seconds.
In order to describe the delay from gust zone to gust zone, a system of multiple delays is defined. The disturbance, which is propagated from gust zone to gust zone, is defined by U_d. The state of the delay at each gust zone X_l^d describes the disturbance acting at each gust zone l. In order to propagate the disturbance through the system, the delay state X_{l-1}^d of the gust zone $l-1$ is the input for the gust zone l. This leads to the delay-system definition:

$$G^d(s) = \begin{cases} X_1^d(s) = e^{-sT_1} U^d(s) \\ X_2^d(s) = e^{-sT_2} X_1^d(s) \\ X_3^d(s) = e^{-sT_3} X_2^d(s) \\ \quad \vdots \\ X_l^d(s) = e^{-sT_l} X_{l-1}^d(s). \end{cases} \tag{25}$$

The time delay from gust zone $l-1$ to gust zone l is described by T_l. Since the transfer function $G^{\text{delay}}(s)$, described in (24), cannot be represented as a rational transfer function a n-th order Padé approximation (26) is applied [10]:

$$e^{-\mathrm{sT}} \approx \frac{(1-\frac{\mathrm{T}}{2\mathrm{n}}s)^{\mathrm{n}}}{(1+\frac{\mathrm{T}}{2\mathrm{n}}s)^{\mathrm{n}}}. \tag{26}$$

The transfer functions in the system $G^d(s)$ (25) are approximated by the Páde formula (26). This results in a system of rational transfer functions $G^d_{approx}(s)$. Hence the downwash at each aerodynamic panel due to a disturbance w^G is

$$w^G_j(s) = T_{jl} G^d_{approx}(s) w^G, \tag{27}$$

where the input w^G is the one-dimensional disturbance signal. Combining (27) and (15) leads to the aerodynamic loads

$$P^G_g(s) = q_\infty T^T_{kg} S_{kj} Q_{jj} T_{jl} G^d_{approx}(s) w^G \tag{28}$$

due to disturbances approximated by the gust zone approach. The transfer function $P^G_g(s)$ is expressed in time domain by the state space model

$$\begin{aligned} \dot{x}_G &= A_G x_G + B_G u \\ y_G &= C_G \cdot x_G + D_G u, \end{aligned} \tag{29}$$

with the output y_G being $y_G = P^G_g$.

4 EQUIVALENT DAMAGE FATIGUE LOADS

In this section a concept enabling the analysis of time history load data with respect to their impact on fatigue is presented. The approach is based on the ideas described in [11–13]. Since the method only makes use of global structural loads, no transformation to stresses is necessary. Hence no material information or component geometries are required. The method assumes that a fatigue failure mode of the structure depends on one specific load, e.g. wing root bending moment. The failure mode is characterized by a P-N curve, similar to a S-N curve, but depending on one global aircraft load instead of stresses. The P-N relation is described by the Basquin relation [14]:

$$P_a = P_U \cdot N^{-\frac{1}{m}}, \tag{30}$$

where P_a is load amplitude and P_U is the ultimate load for which the structure would fail after one cycle. Freebury [12] proposes an P_U equal to $1.5 \cdot P_{max}$ to $4.5 \cdot P_{max}$ with P_{max} being the maximum load within the cases, which are investigated. The exponent m defines the slope of the P-N curve. Freebury [12] proposes an m between 6 and 12. The equivalent damage load is based on the damage accumulation defined by the Pålmgren Miner rule [14]:

$$D^{PM} = \sum_{i=1}^{M} \frac{n_i}{N_i}. \tag{31}$$

The equation relates the fatigue life N_i, measured in cycles, with the corresponding amplitude P_{ai}. Meaning that for example n_1 cycles with a load amplitude P_{a1} and the corresponding fatigue life endurance N_1 leads to the damage $D^{PM}_1 = \frac{n_1}{N_1}$ [12]. The cycle information of the load time history consisting of cycle counts n_i, cycle amplitudes P_{ai} and the corresponding cycle

means P_m. These are derived by the Rainflow counting algorithm (for detailed information about Rainflow counting algorithm the reader is referred to [15]). The P-N curve is defined for a cycle with a mean value of zero, i.e. with a load ration $R = \frac{P_{min}}{P_{max}} = -1$. Since the cycles in a load time history are around a non-zero mean value, the influence of the mean value on the fatigue damage needs to be considered. One method to take the non-zero mean into account is the Goodman rule

$$\frac{P_a}{P_{ai}^c} + \frac{P_m}{P_u} = 1, \tag{32}$$

which relates the cycle amplitude P_a with nonzero mean to a load cycle amplitude P_{ai}^c

$$P_a^c = P_a \frac{1}{\left(1 - \frac{P_m}{P_U}\right)} \tag{33}$$

for the load ratio $R = -1$. This enables the analysis of any load time history using the P-N curve. The cycle amplitudes P_a^c are categorized with respect to their magnitude by the predefined set of bins. This results in the number of cycles n_i for each bin with the amplitude P_{ai}^c . Based on the derived P_{ai}^c the damage D^{PM} is derived according to (31).
The concept of equivalent damage proposes that the damage D_e^{PM} due to the equivalent damage load time history P_e is equal to the damage D^{PM} due to the investigated load time history. The equivalent damage load is characterized by the load amplitude P_{ae}, a defined number of cycles n_e and a corresponding fatigue life N_e. This can be expressed, using the Pålmgren Miner rule, by

$$\sum_{i=1}^{M} \frac{n_i}{N_i} = \frac{n_e}{N_e}, \tag{34}$$

where N_e can be represented by

$$N_e = \left(\frac{P_U}{P_{ae}}\right)^m. \tag{35}$$

Combining (35) with (34) leads to:

$$\underbrace{\sum_{i=1}^{M} \frac{n_i}{N_i}}_{D^{PM}} \stackrel{!}{=} \underbrace{\frac{n_e {P_{ae}}^m}{P_U^m}}_{D_e^{PM}}, \tag{36}$$

which expresses the requirement, that the damage D^{PM} due to the investigated load time history needs to be equal to the damage of the damage equivalent load D_e^{PM}. In order to fulfil (36), it needs to be solved for the unknown P_{ae}. This is achieved by expressing N_i using the Basquin relation (30) and subsequently performing some algebraic transformations leading to:

$$P_{ae} = \left(\sum_{i=1}^{M} \frac{n_i P_{ai}^m}{n_e}\right)^{\frac{1}{m}}. \tag{37}$$

In order to compare two load time histories, e.g. simulated loads with estimated loads, the equivalent fatigue load based on the time-history of the estimation P_{aeEst} and the time-history of the simulation P_{aeSim} are calculated. These two equivalent fatigue loads are set into relation by

$$\eta_E = \frac{P_{aeEst}}{P_{aeSim}}. \tag{38}$$

The coefficient η_E describes the estimation accuracy of the loads estimation system with respect to a failure mode, which is described by a P-N curve.

5 APPLICATION

In this section the proposed workflow is applied to a realistic aircraft model. Since no operational data is available, the sensor data is simulated using an aircraft model similar to the one described in Section 3. First, the setup of the loads estimator is explained. Second, the different scenarios, which the estimator is tested with, are explained. Finally, the results will be provided. The overall loads estimation system is depicted in Figure 7. The estimated loads P_c^{est} are

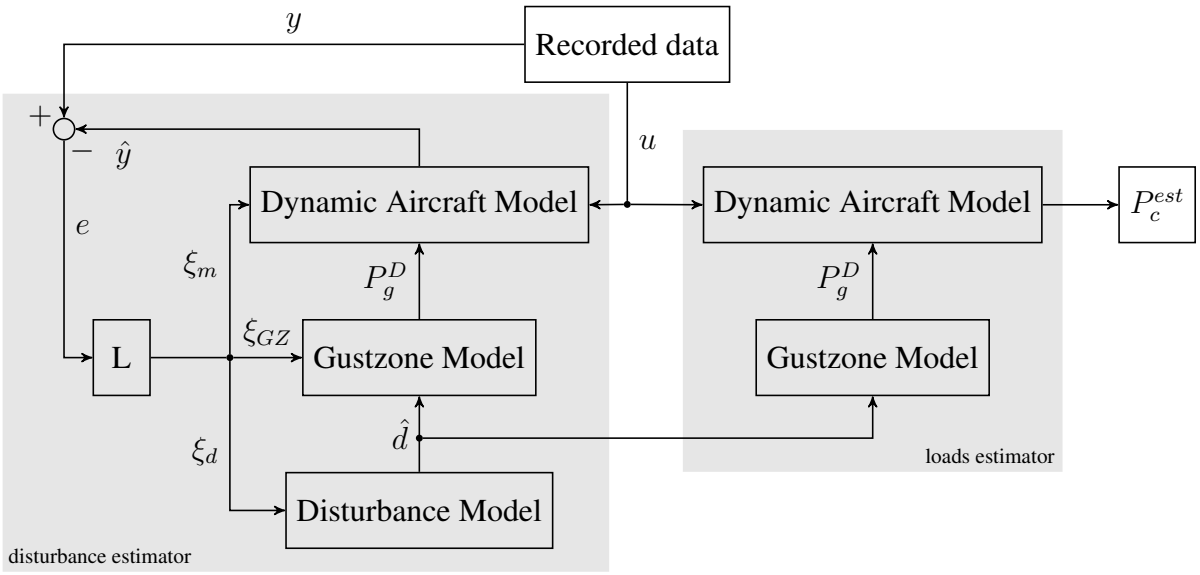

Figure 7: System for loads estimation based on operational data

evaluated by the method of equivalent damage loads as explained in Section 4. As illustrated in Figure 7, the two main blocks are the disturbance estimator and the loads estimation. The disturbance estimator is based on a Kalman-Bucy filter (detailed explanation in Section 2.1) extended by a disturbance estimator as explained in Section 2.2. The general architecture is shown in Figure 3. The system model of the filter consists of the dynamic aircraft model, the gust zone model as well as the disturbance model. The dynamic aircraft model is based on the method described in Section 3. The gust zone model is derived as explained in Section 3.2. In order to be able to estimate the disturbance signal due to the atmospheric disturbances, the disturbance model is implemented according to Section 2.2.

The feedback $\begin{bmatrix}\xi_m & \xi_{GZ} & \xi_d\end{bmatrix} = L \cdot e$ influences the state derivatives $\dot{\hat{x}}$ of the dynamic flexible aircraft model, disturbance model as well as the gust zone model by ξ_m, ξ_{GZ} and ξ_d. Especially the state derivatives of the system model $\dot{x} = \begin{bmatrix}\ddot{u}_b & \ddot{u}_f & \ddot{u}_f\end{bmatrix}$ are directly influenced due to ξ_m, according to (2). This influence leads to inertia loads (20) due to ξ_m without any external loads P_g^{ext} acting on the aircraft structure. This violates Newton´s third law [16], actio equals to reactio, because the inertia loads (reactio) is missing it´s counterpart (actio). As a result, the derived loads by the force summation method (19) would be incorrect.

Therefore, only the disturbance estimation w^D is extracted and the cut loads P_c^{est} are derived in the separate loads estimation block as depicted in Figure 7.

The loads estimator consists of a gustzone model as well as a dynamic flexible aircraft model. The loads estimator inputs are the estimated w^D from the disturbance estimator as well as the recorded control inputs u. This results in the estimated cut loads P_c^{est} for the whole aircraft structure. Afterwards, the cut loads P_c^{est} are processed by the method of EDL as explained in Section 4. This allows a comparison between the reference, the simulated loads and the estimated loads with respect to the impact on fatigue. The loads estimator is tested for discrete

gust (1-cos) as well as continuous turbulence (CT) events. These events are investigated at one flight point defined by constant Mach number and altitude. The recorded data contains sensor data generated with a non-linear dynamic flexible aircraft model as described in 3. In order to analyze the performance of the estimator with uncertainties in the aerodynamics due to neglecting unsteady effects, the data is generated using both VLM and DLM for the modeling of the aerodynamic loads. The influence of steady and unsteady aerodynamics on the loads estimation are investigated for continuous turbulence load cases. Additionally, the performance of the estimator is evaluated with discrete gust (1-cos shape) load cases.
For the defined cases the EDL criteria is evaluated for the right wing for the quantities F_z (shear force normal to wing reference surface), M_x (bending moment) and M_y (torsion moment). The corresponding coordinate systems are displayed in Figure 5.

5.1 Continuous turbulence analysis

The simulation of continuous turbulence in the time domain is based on the Dryden spectrum:

$$\Phi_w(\Omega) = \sigma_w^2 \frac{L_w}{\pi V} \frac{1 + 3(L_w \frac{\omega}{V})^2}{(1 + (L_w \frac{\omega}{V})^2)^2}, \tag{39}$$

where L_w is the turbulence scale length, σ_w the root mean square (RMS) of the turbulence intensity and $\frac{\omega}{V}$, the spatial frequency. The turbulence scale length σ_w depends on the altitude and probability of exceedance. This relation is illustrated in Figure 8. The lines in Figure 8 represent constant levels of probability of exceedance [17]. The advantage of the Dryden spectrum is that a continuous filter can be designed to convert a white noise time history signal to a time signal with a spectral shape similar to the one defined in (39) [18]. In this paper the loads due to continuous turbulence in vertical direction are investigated. For this investigation the parameter "probability of exceedance", which influences σ_w and L_w of the Dryden spectrum (39) and therefore the amplitude and strength of the loads acting on the aircraft, is varied

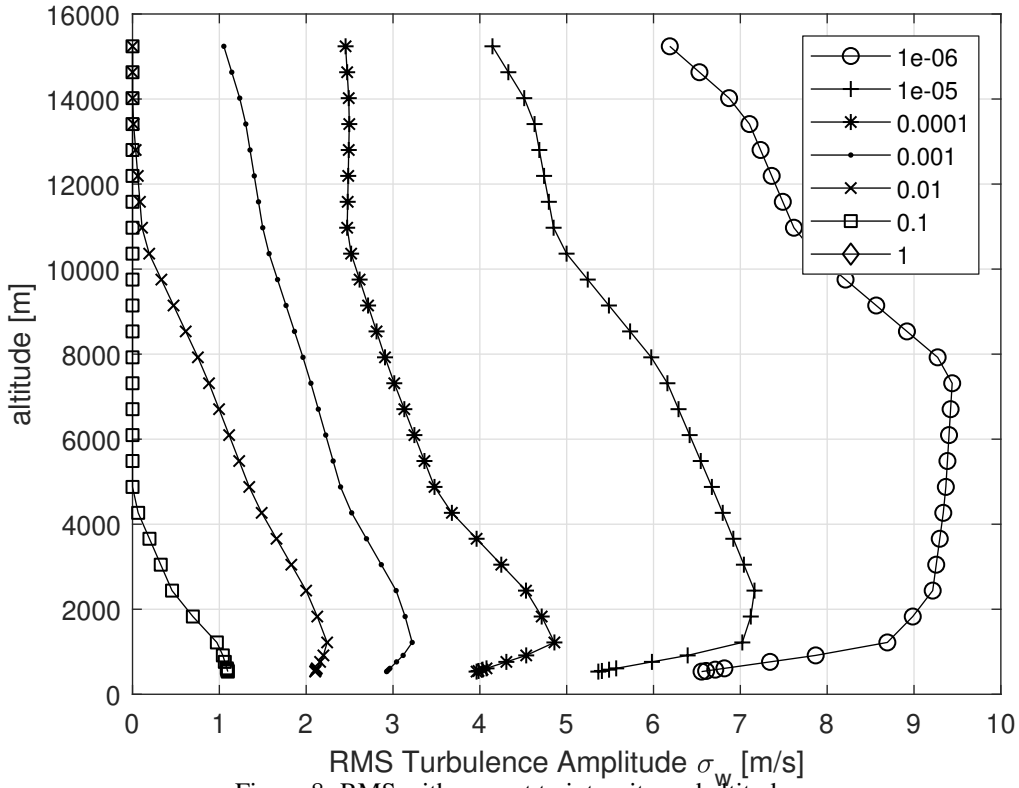

Figure 8: RMS with respect to intensity and altitude

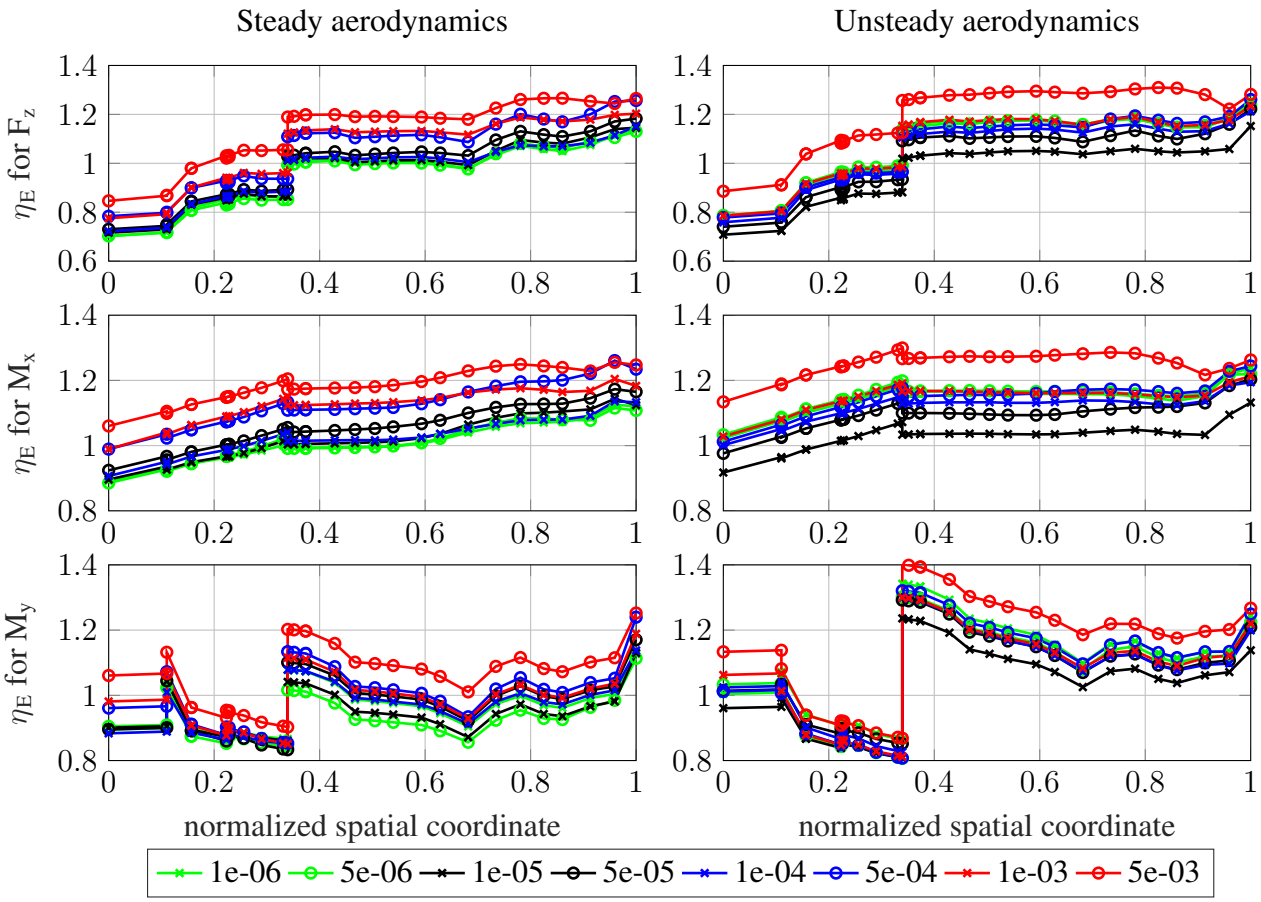

Figure 9: Comparison of η_E for right wing loads for continuous turbulence cases with different probabilities of exceedance with reference VLM and DLM

between 1×10^{-6} and 5×10^{-3}. The simulations are conducted at one specific Mach-number and altitude. As described above, the recorded data is generated using the steady aerodynamics, hence VLM, as well as unsteady aerodynamics, hence DLM.
In Figure 9 the resulting η_E, defined in (38), is derived for each monitoring point for the internal structural loads F_z, M_x and M_y on the right wing. The x-axis of the plot is the spatial coordinate of the analysis points normed by the maximum absolute spatial coordinate. Translated for the right wing, it means that the spanwise coordinate is normalized by the half-span. For the steady as well as the unsteady investigation, F_z shows an underestimation of the EDL for the inner wing up to the spatial coordinate of ≈ 0.35. Here a jump to $\eta_E \geq 1$ occurs, i.e., the EDL is overestimated. Due to a strong dependence of the wing bending moment M_x of F_z, η_E shows a similar shape like F_z, but shifted in y-direction. For M_y, η_E varies between ≈ 0.8 and ≈ 1.2. The analysis with respect to the probability of exceedance shows a tendency of overestimation, the higher the probability of exceedance is.

5.2 Discrete gust analysis

The velocity profile v_g of the discrete gust (1-cos shape) is defined by the certification requirements in CS/FAR 25.341 [19].

$$v_g = \frac{1}{2} U_0 \left(1 - \cos\left(\frac{2\pi x_j}{2H}\right)\right) \tag{40}$$

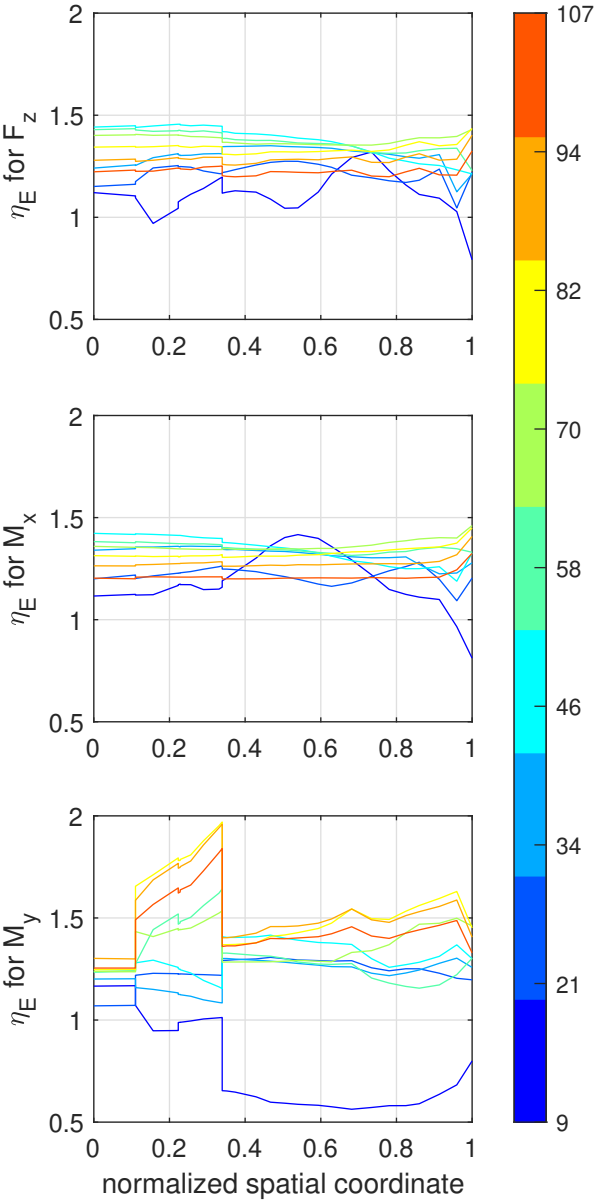

Figure 10: Comparison of η_E for right wing loads generated with VLM aerodynamics

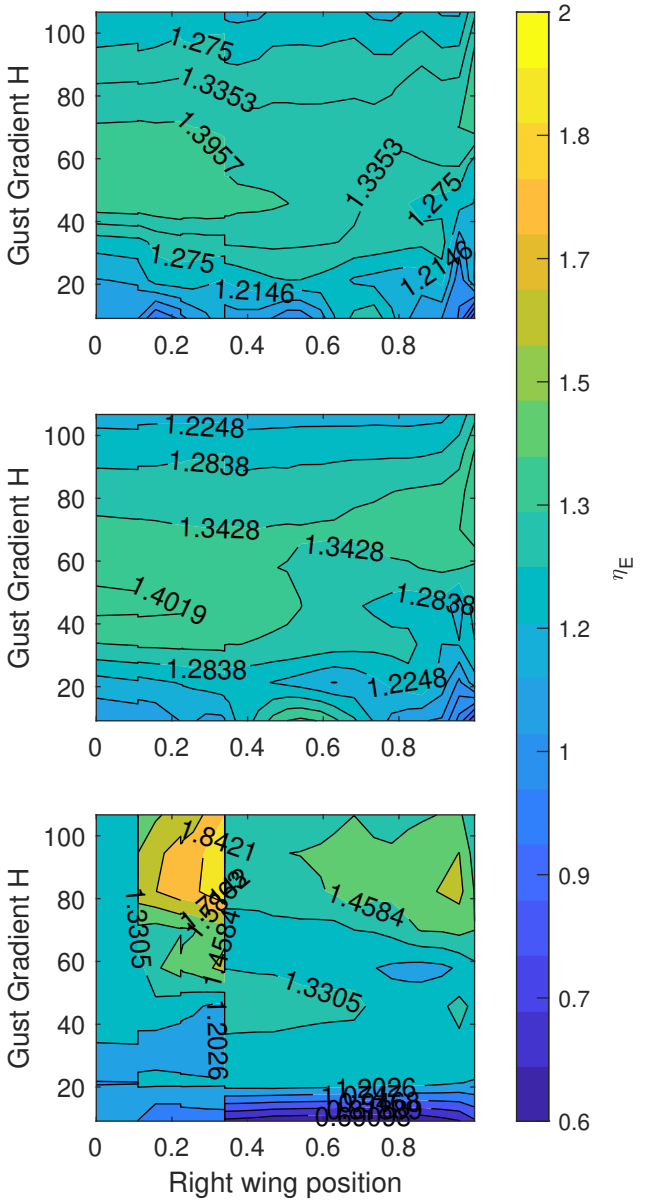

Figure 11: Contour plot of η_E for different gust gradients on right wing

The parameter x_j describes the relative position of each aerodynamic panel with respect to the gust. The design gust velocity U_0, hence the gust amplitude, as well as the gust gradient H are defined according to CS/FAR 25.341 [19]. For a more detailed explanation of the implementation the reader is referred to [8]. The gust gradient represents the distance parallel to the flight path from the beginning to the peak of the gust. In the certification H is defined for 9 m to 107 m. The refence data is generated simulating the load cases using a model with VLM. The simulated cases vary in gust gradient length. For the investigation one Mach-number and one altitude is chosen. In total 9 different gust gradients equally distributed between 9 m and 107 m are investigated. Figure 10 shows η_E for the loads F_z, M_x and M_y for the right wing with respect to the normalized spatial coordinate. The plot shows that η_E is overestimated by the loads estimator for all gust lengths, except for the shortest investigated length with $H \approx 9$ m. Here η_E is significantly underestimated for the middle to outer wing for M_y. This gust length

also shows significant variation for F_z and M_y, while the shape of the curve clearly differs from the results for the other gust lengths.
For better visualization of η_E with respect to the gust gradients H and the normalized spatial coordinate, a contour plot is presented in Figure 11. The x-axis is again the spatial coordinate. The y-axis characterizes the different gust gradients. The η_E is characterized by the color and the level lines. The color bar next to the plot describes the numerical quantification of the colormap. The figure shows the largest overestimation for F_z and M_x at the inner wing for gust gradients between $H = 40\,\text{m}$ and $H = 80\,\text{m}$. For M_y the biggest overestimation also occurs for the inner wing. quantitatively, the overestimation for M_y is larger than for F_z and M_x.

6 CONCLUSIONS

A toolchain enabling the estimation of loads due to vertical atmospheric disturbances from sensor data typically provided by avionics system of an airliner is presented. The estimator is based on a Kalman-Bucy filter architecture. A mathematical description of a dynamic flexible aircraft model is used within the estimator. It is assumed that the occurring disturbances consist of continuous turbulence as well as discrete gusts. The results of the estimator and the simulation are compared using the equivalent damage load concept. For the continuous turbulence the estimations show an error with respect to the EDL criteria of $\approx \pm 25\%$. The loads are both under and overestimated with respect to EDL. For the discrete gust, the estimates differ with up to $\approx +50\%$ for F_z and M_x while for M_y the error lies in a range of $\approx +100\%$ with respect to the EDL criteria.
As next steps more uncertainties shall be investigated, e.g. uncertainties in the structural model like stiffness, mass distributions and control effectiveness. A further aspect will be the validation of the approach with real sensor data to be able to tackle aspects as realistic sensor noise and sampling rates.

7 ACKNOWLEDGMENT

This work is performed within the framework of the German national research project INTELWI.

8 REFERENCES

[1] Boller, C. and Buderath, M. (2007). Fatigue in aerostructures–where structural health monitoring can contribute to a complex subject. *Philosophical transactions. Series A, Mathematical, physical, and engineering sciences*, 365(1851), 561–587. ISSN 1364-503X. doi:10.1098/rsta.2006.1924.

[2] Schmuecker M., Meyer H. J., and Ladda V. (04061987). New approaches in the field of inflight load evaluation. In *28th Structures, Structural Dynamics and Materials Conference*. Reston, Virigina: American Institute of Aeronautics and Astronautics, p. 1971. doi:10.2514/6.1987-848.

[3] Hunt, S. R. (2001). *Validation of the eurofighter typhoon structural health and usage monitoring system*.

[4] H. Henrichfreise, L. Bensch, J. Jusseit, L. Merz, M. Gojny (2009). Estimation of gusts and structural loads for commercial aircraft. In *International Forum on Aeroelasticity and Structural Dynamics (IFASD) 2009*.

[5] Montel, M. (2018). *Hybride Beobachter-Methode zur Strukturlastüberwachung und deren Validierung mit Flugversuchsdaten*. Dissertation, Technische Universität Hamburg and Shaker Verlag GmbH.

[6] Simon, D. (2006). *Optimal state estimation: Kalman, H [infinity], and nonlinear approaches*. Hoboken, NJ: Wiley-Interscience. ISBN 9780471708582. doi: 10.1002/0470045345.

[7] Hofstee, J., Kier, T., Cerulli, C., & Looye, G (2003). A variable, fully flexible dynamic response tool for special investigations (varloads). In *International Forum on Aeroelasticity and Structural Dynamics (IFASD) 2003*.

[8] Kier, Thiemo M., and Gertjan Looye (2009). Unifying manoeuvre and gust loads analysis models.

[9] Wright, J. R. and Cooper, J. E. (2015). *Introduction to aircraft aeroelasticity and loads*. Aerospace series. Chichester, West Sussex, United Kingdom: Wiley, second edition ed. ISBN 978-1-118-48801-0.

[10] Skogestad, S. and Postlethwaite, I. (2001). *Multivariable feedback control: Analysis and design*. Chichester: Wiley, reprinted. ed. ISBN 0471942774.

[11] Sutherland, H. J. On the fatigue analysis of wind turbines. doi:10.2172/9460.

[12] Freebury, G. and Musial, W. (2000). Determining equivalent damage loading for full-scale wind turbine blade fatigue tests. In *2000 ASME Wind Energy Symposium*. Reston, Virigina: American Institute of Aeronautics and Astronautics. doi:10.2514/6.2000-50.

[13] Ossmann, D., Seiler, P., Milliren, C., et al. (2021). Field testing of multi-variable individual pitch control on a utility-scale wind turbine. *Renewable Energy*, 170(2), 1245–1256. ISSN 09601481. doi:10.1016/j.renene.2021.02.039.

[14] Schijve, J. (2009). *Fatigue of Structures and Materials*. Dordrecht: Springer Netherlands. ISBN 9781402068072. doi:10.1007/978-1-4020-6808-9.

[15] E08 Committee. Practices for cycle counting in fatigue analysis. doi:10.1520/E1049-85R17.

[16] Rajapakse, N. (2009). *Engineering Mechanics 1: Statics*. SpringerLink Bücher. Berlin, Heidelberg: Springer Berlin Heidelberg. ISBN 978-3-540-89936-5. doi:10.1007/978-3-540-89937-2.

[17] Department of Defense (1997). Mil-hdbk-1797, flying qualitites of piloted aircraft.

[18] Hoblit, F. M. (1988). *Gust Loads on Aircraft: Concepts and Applications*. Washington DC: American Institute of Aeronautics and Astronautics. ISBN 978-0-930403-45-4. doi: 10.2514/4.861888.

[19] European Union Aviation Safety Agency (15.12.2020). Certification specifications and acceptable means of compliance for large aeroplanes: Cs-25.